Thermal diffusion and Soret feedback of gold-doped polyorganosiloxane nanospheres in toluene

R. Spill and W. Köhler*
Physikalisches Institut, Universität Bayreuth, D-95440 Bayreuth, Germany

G. Lindenblatt and W. Schaertl
Institut für Physikalische Chemie, Universität Mainz, D-55099 Mainz, Germany

(Received 6 June 2000)

We have investigated diffusion and thermal diffusion properties of light-absorbing colloidal polyorganosiloxane microgels containing tiny nanometer-sized gold clusters dispersed in toluene. Transient holographic gratings allow for very subtle perturbations in the linear regime where Soret feedback is negligible. Gold-doped colloids of different size and crosslink ratios show different Soret coefficients but identical thermal diffusion coefficients D_T. Undoped colloids tend to aggregate, but a consistent interpretation is obtained if an identical D_T is assumed for the doped, the undoped, and the aggregated particles. Previously reported Soret feedback measurements on similar systems incidentally yielded comparable Soret coefficients. We show, however, that they suffer from strong convective perturbations.

PACS number(s): 82.70.Gg

I. INTRODUCTION

Recently, dynamic light scattering experiments on gold-doped polyorganosiloxane microgels in solution have been carried out (Schaertl and Roos [1]). These colloids are different from systems usually studied by light scattering due to their ability to absorb light at the wavelength of the laser. The resulting heating of the solution triggers convection, which leads to a characteristic beating of the time correlation function of the scattered light intensity at high laser powers.

An interesting property of such light-absorbing colloids is that they can undergo thermal diffusion within the nonuniform temperature distribution created by the absorbed laser beam. If the laser heating and the Soret coefficient are sufficiently high, the redistribution of the absorbers in turn modifies the absorption properties and, hence, the heat release. This nonlinear Soret feedback can be positive if the colloids migrate into the heated volume, or negative if they migrate towards the colder regions. In the first case, the feedback is self-amplifying; in the second case, it limits the maximum heat release in the sample. Depending on the sign of the Soret coefficient and on the refractive index increment $(\partial n/\partial c)_{p,T}$, self-focusing or defocusing can be observed. These effects have been discussed by Tabiryan and Luo [2], and experiments have been reported by Freysz *et al.* [3] and by Du and Luo [4].

In Ref. [1] this feedback has been utilized to determine the Soret coefficient of the microgels from the nonlinear power dependence of the phase shift at the center of the transmitted laser beam. Unfortunately, this procedure, which is based on the theory developed by Tabiryan and Luo [2], does not account for convection. Since convection is dominant in these experiments, the reported Soret coefficients are presumably not correct.

In this paper we first discuss the influence of convection on the Soret feedback experiments reported in Ref. [1]. Then, we reexamine diffusion and thermal diffusion properties of such microgels with and without gold nuclei. To avoid problems associated with convection, we resort to the transient holographic grating technique of thermal diffusion forced Rayleigh scattering (TDFRS) [5–7]. This technique is not only insensitive to convection but also avoids nonlinear effects, since it induces only very subtle concentration changes.

Soret feedback is, however, not the only reason to shine light on thermal diffusion of these colloids. A comparison between doped and undoped microgels and aggregates thereof would give information about whether the gold nuclei themselves and the formation of aggregates have any influence on the thermal diffusion coefficient.

While the mass diffusion coefficient of polymers and colloids depends on their size in a well known way, the situation is not so clear for the thermal diffusion coefficient D_T. For linear, branched, and star polymers, it is well established that D_T is molar mass independent [8–10]. For highly crosslinked polystyrene microgels in toluene, the same D_T as for the linear polymer has been found [11]. For heterogeneous systems, such as block copolymers [12] and micelles [13], it has been shown that D_T is determined by the species occupying the outer surface, where the particle-solvent contact takes place. In contrast to these results is the size dependence of D_T for suspensions of colloidal particles, as reported by Jeon *et al.* [14]. Since we have synthesized the microgels with two different sizes, we can also contribute to this interesting and still open question, as to which parameters influence D_T of a colloidal system.

II. EXPERIMENTAL

A. Synthesis of microgels

Synthesis of organosilicon microgels loaded with tiny gold clusters has been described previously [15]. These cross-linked spherical nanoparticles of average radius 10–40 nm are formed by polycondensation of trimethoxysilanes and

*Author to whom correspondence should be addressed. Email address: werner.koehler@uni-bayreuth.de

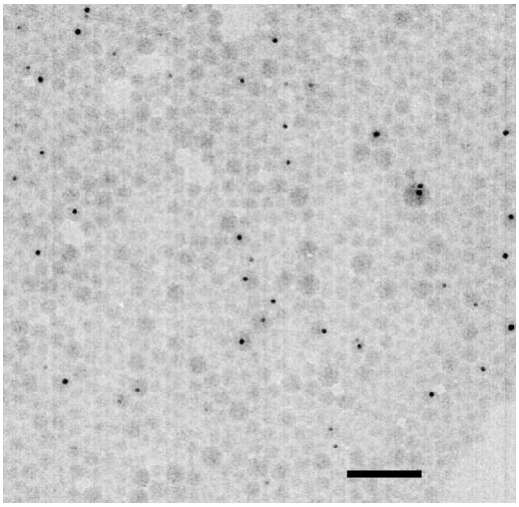

FIG. 1. Transmission electron micrograph of the gold labeled microgels. Only a fraction of the spheres is loaded with tiny gold clusters. Scale bar 100 nm.

dimethoxysilanes in microemulsion. The crosslink density of the microgels is adjusted via the content of bifunctional and trifunctional silane monomers, respectively. The gold clusters themselves are prepared by *in situ* reduction of the metal salt $HAuCl_4$ by SiH within the microgel network. Reaching a certain size, the gold clusters become trapped within the crosslinked microgels. Samples used in this study are named *g*50/50 and *n*50/50. Here, *g* corresponds to particles reacted with HAuCl4 and therefore labeled with gold clusters. Particles named *n* are identical microgels without any gold clusters. 50/50 corresponds to a 1:1 mixture of bifunctional and trifunctional silanes. The microgels have a core-shell topology (see [15]), i.e., a core containing the Si-H moieties used for reduction of the gold salt, and a surrounding shell without Si-H groups.

The core is formed by cocondensation of the trifunctional silanes $HSi(OCH_3)_3$ and $CH_3Si(OCH_3)_3$ with the bifunctional silane $(CH_3)_2SI(OCH_3)_2$, whereas the shell consists only of $CH_3Si(OCH_3)_3$ and $(CH_3)_2Si(OCH_3)_2$. For particles used in these studies, both core and shell had identical crosslink densities.

B. Microgel characterization and measurement of transport coefficients

Figure 1 shows a transmission electron micrograph of the gold labeled particles. The tiny dark spots are the gold clusters, which are surrounded by the organosilicon network. Size polydispersity of these particles as determined from size exclusion chromatography, which has been calibrated for absolute particle radii of organosilicon microgels by light scattering (see [16]), was approximately 30%. The average particle radius R_h as measured by dynamic light scattering, using an ALV 3000 correlator and a Kr-laser at 647.1 nm wavelength and laser power less than 100 mW (to avoid convection due to light absorption), was 19 nm. A second sample of identical *g*50/50 topology with slightly larger particle radius $R_h = 25$ nm was also used during these studies (see below).

TDFRS measurements were carried out as described in previous publications [17,18]. For enhanced sensitivity and robustness against perturbations, a heterodyne detection scheme with active phase tracking was employed. An argon ion laser (Spectra Physics 2020, 488 nm) was used for writing and a helium-neon laser (NEC, 35 mW, 632.8 nm) for readout of the grating. The diffracted beam was coupled into a single mode optical fiber to suppress incoherent background. The fringe spacing of the grating was of the order of 10 μm. The refractive index increments $(\partial n/\partial c)_{p,T} = -0.060 \pm 0.002$, where c is the concentration in weight fractions, and $(\partial n/\partial T)_{p,c} = (-5.62 \pm 0.01) \times 10^{-4}$ K^{-1} were determined interferometrically [19]. All measurements were performed at room temperature. Solutions were prepared with high-quality toluene (Merck, pro analysi).

III. REEXAMINATION OF NONLINEAR SELF-INDUCED PHASE MODULATION

In this section we reexamine the self-induced phase modulation experiments from Ref. [1] and discuss similar unpublished measurements on the here discussed gold-doped nanospheres in toluene. In these experiments, a laser beam is used to induce a thermal lense due to slight absorption in the sample. Redistribution of the nanospheres within the nonuniform temperature profile changes the absorption, and, hence, the heat insertion into the sample. This nonlinear effect is known as Soret feedback [2] and eventually limits the heat insertion into the system if the sign of the Soret coefficient is such that the absorbing particles migrate out of the regions heated by the laser beam (negative feedback) [3]. The nonlinear power dependence of the on-axis phase shift of the transmitted beam is used to estimate the Soret coefficient.

To account for Soret feedback, Tabiryan *et al.* [2] start in the usual way with the heat equation for the temperature T,

$$\frac{\partial T}{\partial t} = D_{th}\Delta T + \frac{\sigma I}{\rho c_p}. \tag{1}$$

D_{th} is the thermal diffusivity, I the laser intensity, ρ the density, c_p the specific heat at constant pressure, and σ the absorption coefficient of the liquid.

An extension of Ficks second law of diffusion is employed to couple the concentration to the temperature profile:

$$\frac{\partial c}{\partial t} = D\Delta c + D_T c(1-c)\Delta T. \tag{2}$$

D and D_T are the mass diffusion and the thermal diffusion coefficient, respectively.

Soret feedback is introduced by linking the absorption coefficient, and hence the source term in the heat equation [Eq. (1)], to the concentration of the absorbers,

$$\sigma = c\varepsilon. \tag{3}$$

ε is the extinction coefficient of the solute per concentration unit (here mass fraction).

For cylindrical geometry, the problem becomes two dimensional in the limit of infinite path length, and heat transport through the cuvette windows in the direction of the optical axis can be neglected. The magnitude of the nonlinear feedback is controlled by the dimensionless parameter

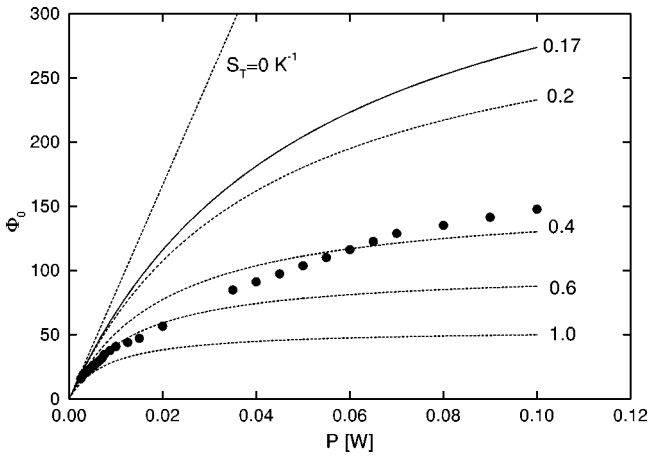

FIG. 2. Phase shifts Φ_0 at the center of the transmitted beam as measured and calculated from Eq. (5) for different Soret coefficients S_T.

$$\eta = \frac{\sigma_0 S_T P}{\pi \lambda_T}. \tag{4}$$

$S_T = D_T/D$ is the Soret coefficient. σ_0 is the equilibrium absorption coefficient for uniform sample temperature, P the total laser power, and λ_T the thermal conductivity of the solution. Interestingly, the power and not the intensity appears in Eq. (4).

The on-axis phase shift of the transmitted laser beam is given by

$$\Phi_0 = -\frac{2\pi L}{\lambda}\left[c_0\left(\frac{\partial n}{\partial c}\right)_{p,T} - \frac{1}{S_T}\left(\frac{\partial n}{\partial T}\right)_{p,c}\right]\frac{\eta}{1-\eta}. \tag{5}$$

Note that the factor c_0 in front of $(\partial n/\partial c)_{p,T}$ is missing in Eq. (48) of Ref. [2] and in Eq. (10) of Ref. [1]. L is the cuvette path length, λ the laser wavelength, and n the index of refraction of the solution. Nonlinearities can be neglected as long as $\eta \ll 1$.

In Ref. [1] the derivatives of the refractive index were not known and the factor

$$K = -\frac{2\pi L}{\lambda}\left[c_0\left(\frac{\partial n}{\partial c}\right)_{p,T} - \frac{1}{S_T}\left(\frac{\partial n}{\partial T}\right)_{p,c}\right] \tag{6}$$

was treated as an unknown. The other unknown was the Soret coefficient S_T, which was estimated from the nonlinear power dependence of Φ_0 to $S_T = 0.06$ and $0.07\ \mathrm{K}^{-1}$ for particles of 75 and 50 nm diameter, respectively. The same procedure yields for the $g50/50$ microgels discussed here a power-dependent Soret coefficient, whose extrapolation to zero laser power gives $S_T \approx 0.20\ \mathrm{K}^{-1}$. This result agrees remarkably well with the TDFRS results (see below), but we will show in the following that the experiment is dominated by convection. Convection is, however, not accounted for in the data analysis based on an estimation of η [Eq. (4)], as proposed in [2].

For the microgels in toluene discussed here, both refractive index increments $(\partial n/\partial c)_{p,T}$ and $(\partial n/\partial T)_{p,c}$ are known, and Φ_0 can be calculated according to Eq. (5). Figure 2 shows the on-axis phase shift as a function of laser power for different values of S_T together with data measured for $g50/50$ ($c_0 = 2$ g/L, $\sigma_0 = 0.50\ \mathrm{cm}^{-1}$, $\lambda_T = 0.131\ \mathrm{W(mK)}^{-1}$, $L = 1.0$ cm, $\lambda = 514$ nm).

Evidently, the power dependence of the measured phase shift is highly nonlinear, but it cannot be described by Eq. (5) assuming a constant S_T. A clear indication that the nonlinearity is not caused by a Soret-driven bleaching of the absorption but rather by a cooling of the sample within the laser path by convection is the deformation of the concentric interference patterns of the transmitted beam at high laser powers in Fig. 12 of Ref. [1].

With $S_T = 0.17\ \mathrm{K}^{-1}$ (see Sec. IV), we obtain

$$\left|c_0\left(\frac{\partial n}{\partial c}\right)_{p,T}\right|\left|\frac{1}{S_T}\left(\frac{\partial n}{\partial T}\right)_{p,c}\right|^{-1} = 0.036 \tag{7}$$

for the ratio between the concentration and the temperature contribution in Eq. (6). Hence, the asymmetric interference pattern in this figure is essentially caused by a thermal lense, and not by a concentration lense, and it must be concluded that the volume within the beam path is exchanged by convective currents on a time scale comparable to the heat diffusion time. On the other hand, heat diffusion is more than 3 orders of magnitude faster than mass diffusion. Hence, there is no time for a concentration change to build up that would lead to a nonlinear Soret feedback. For a more quantitative estimation of the influence of convection it is necessary to determine the relevant time scales.

There is no unique definition of the mass diffusion time τ and the heat diffusion time τ_{th}. For simplicity, we define τ as the time after which the on-axis concentration c of an initially within a cylinder of radius a homogeneously distributed diffusing species has decayed by 50%. According to Ref. [20], c decays from its initial value c_0 like

$$c = c_0(1 - \mathrm{e}^{-a^2/(4Dt)}). \tag{8}$$

Hence,

$$\tau = \frac{a^2}{4D \ln 2} \quad \text{and} \quad \tau_{th} = \frac{a^2}{4D_{th} \ln 2}. \tag{9}$$

The corresponding convection time is the time needed for a volume element to flow through the cylinder in the direction of gravity, perpendicular to the optical (cylinder) axis,

$$\tau_c = \frac{2a}{v_c}. \tag{10}$$

The power dependence of the convective velocity v_c within the scattering volume was determined in Ref. [1] from the characteristic beating of the intensity autocorrelation function in PCS measurements: $v_c/P \approx 0.3\ \mathrm{cm/(s\,W)}$.

Soret feedback can only be expected to dominate if the characteristic mass diffusion time τ is shorter than the characteristic time scale for convection τ_c. Since τ and τ_{th} depend quadratically on a, whereas τ_c depends only linear on a, Soret feedback should dominate for small beam waists, convection for large ones. The scenario is summarized in Fig. 3 with $D = 2.4 \times 10^{-7}\ \mathrm{cm^2/s}$ and $D_{th} = 8.9 \times 10^{-4}\ \mathrm{cm^2/s}$. The dashed lines with slope one correspond to the

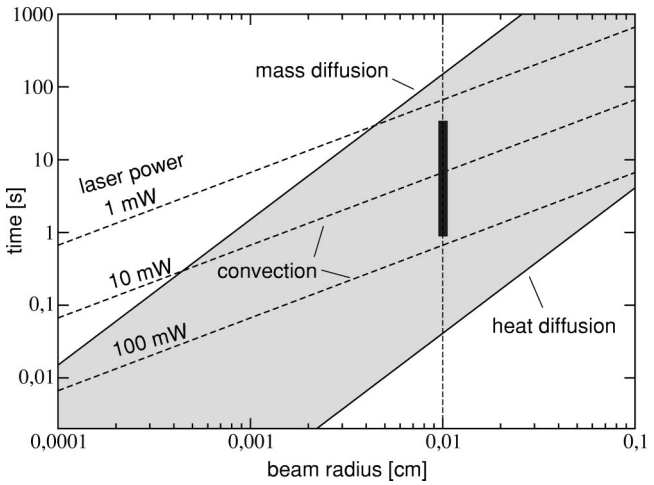

FIG. 3. Relevant time scales of the Soret feedback experiment as a function of the radius of the laser beam. The bar indicates the parameter range of the measurements from Fig. 2.

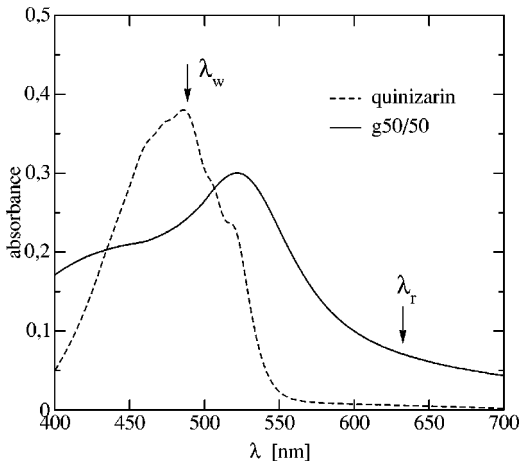

FIG. 4. Absorption spectra of gold-doped nanospheres ($g50/50$, $c=1.078\times10^{-2}$) and quinizarin ($c=8.5\times10^{-6}$) in toluene. Writing wavelength $\lambda_w=488$ nm and readout wavelength $\lambda_r=632.8$ nm. Path length 1 mm.

convection times for different laser powers. The beam waist after a lense with focal length of $f=30$ cm is approximately $2a=4\lambda f/(\pi d)\approx200$ μm for a beam with initial diameter $d=1.2$ mm. The bar in Fig. 3 symbolizes the parameter range of the measurements. Even for the lowest laser powers employed, the experiment is still dominated by convection. The reasonable agreement of the thus determined Soret coefficients with the ones discussed in the following section is merely a coincidence.

IV. MEASUREMENT OF TRANSPORT COEFFICIENTS BY TDFRS

Because of the problems associated with convection in the Soret feedback experiments discussed in the preceding sections, we resorted to TDFRS, for which it had been shown in [17] that convection does not play a role in a well-designed experiment.

In TDFRS experiments reported so far, the absorption of the liquid mixture or polymer solution has always been negligible at the writing wavelength for the holographic grating (488 nm) [5–7,10,21–23], and some dye, e.g., quinizarin, had to be added to enhance absorption of light for the formation of a temperature grating. The sole function of the dye is the thermalization of energy from the incident radiation. Otherwise it must be inert, not undergo any photoreaction, and not be redistributed within the temperature grating by thermal diffusion or some other mechanism.

The situation is quite different for the gold-doped nanospheres, which show significant absorption at the writing wavelength (488 nm) and even some absorption at the readout wavelength (632.8 nm). Their absorption spectrum in toluene is shown in Fig. 4 together with the spectrum of quinizarin in the same solvent.

A. Influence of Soret feedback

At higher concentrations, the measurements were conducted with the pure solution. At lower concentrations, absorption was enhanced by addition of some dye, like in case of nonabsorbing samples. It is not immediately evident whether standard TDFRS experiments give the correct Soret and thermal diffusion coefficients or whether Soret feedback must be taken into account. Hence, we first will discuss various experimental boundary conditions and estimate the importance of nonlinear feedback.

The cuvettes employed for the holographic experiment have rectangular windows of 20×4 mm^2, which are oriented perpendicular to the optical axis. The thickness of the liquid layer between the two windows is 200 μm. The optical density of the sample was always below 0.4, laser powers ranged from 25 to 80 mW, with beam diameters of approximately 6 mm. Following Ref. [17], the relative concentration change within the 10 μm periodicity of the grating can be estimated to be below 10^{-4} for Soret coefficients of the order of 0.1 K^{-1}, as found for the nanospheres in toluene (see below). Hence, nonlinear effects within the holographic grating are completely negligible.

More serious concerns may arise with respect to redistribution of the solute on a much larger length scale of several millimeters, namely within the Gaussian intensity distribution of the laser beam and between the laser spot and the not illuminated cuvette volume. While such a concentration change does not directly interfere with the modulation within the grating because of the very different diffusion lengths, it leads to errors in the average concentration within the probed volume and, as a consequence, to wrong Soret coefficients. This argument also holds for nonabsorbing solutes and solvents with added dye. The temperature rise δT_s of the whole illuminated spot has been estimated in Ref. [17] as a few hundred millikelvin, limited by the rather efficient heat transport through the thin liquid layer and the cuvette windows. Again, the resulting concentration changes

$$\frac{\delta c_s}{c}\approx S_T\delta T_s\approx10^{-2} \tag{11}$$

can be neglected.

In summary, Soret feedback can be neglected for the TDFRS measurements. It becomes important for thick samples, as employed in Ref. [1]. However, as outlined in

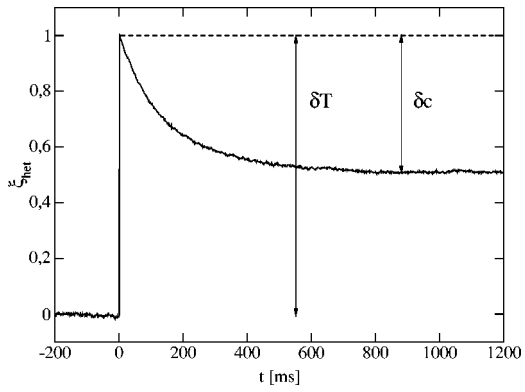

FIG. 5. Normalized heterodyne diffraction efficiency of $g50/50$ in toluene, $c=1.078\times10^{-2}$.

the preceding section, these measurements are not dominated by Soret feedback but rather by convection.

B. Gold-doped microgels

The TDFRS experiment is straightforward and has been described in previous publications [7,17,24]. Taking the power absorbed from the optical interference grating as the source term for the heat equation, a temperature grating builds up within the sample, which, due to the Ludwig-Soret effect, induces a superimposed concentration grating. The diffraction efficiency $\zeta_{het}(t)$ of the resulting refractive index grating is read in a heterodyne experiment.

Since the heat diffusion time $\tau_{th}=(D_{th}q^2)^{-1}$ and the mass diffusion time $\tau=(Dq^2)^{-1}$ are well separated, $\tau\approx10^3\tau_{th}$, it is sufficient for our purpose to neglect τ_{th} and assume an instant response of the temperature grating. D_{th} is the thermal diffusivity, D the mass diffusion coefficient, $q=2\pi/d$ is the absolute value of the grating vector, and d the fringe spacing of the grating. Neglecting, as usual, the Dufour effect, the working equation for the heterodyne diffraction efficiency, normalized to the thermal signal, for a solution of monodisperse particles in response to a step-like excitation at $t=0$ is

$$\zeta_{het}(t)=1-\frac{(\partial n/\partial c)_{p,T}}{(\partial n/\partial T)_{p,c}}c_0(1-c_0)S_T(1-e^{-t/\tau}). \quad (12)$$

Figure 5 shows the normalized heterodyne diffraction efficiency for $g50/50$ at a concentration of $c=1.078\times10^{-2}$ in toluene. After the fast rise of the signal stemming from the temperature grating, there is the slow contribution from the concentration grating, which reduces the initial diffraction efficiency. Because of the negative value of $(\partial n/\partial c)_{p,T}$, this decrease corresponds to a positive Soret coefficient: the solute migrates towards the cooler regions.

1. Soret coefficients

Figure 6 shows the normalized steady-state amplitudes of the concentration signal in Eq. (12),

$$A=\frac{(\partial n/\partial c)_{p,T}}{(\partial n/\partial T)_{p,c}}c_0(1-c_0)S_T, \quad (13)$$

as a function of concentration for $g50/50$.

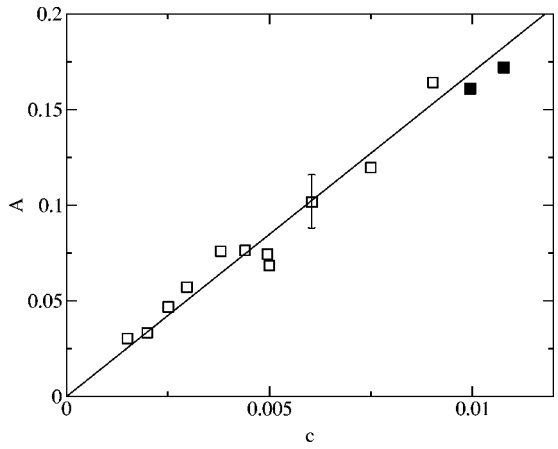

FIG. 6. Amplitude of the concentration signal as a function of concentration for $g50/50$. The solid points have been obtained without additional dye.

For such small concentrations below 1%, $c_0(1-c_0)\approx c_0$, and the Soret coefficient $S_T=0.17\ \mathrm{K}^{-1}$ is obtained from the linear slope. The two data points corresponding to the highest concentrations have been measured without added dye. For the lower concentrations, some quinizarin has been added. Obviously, there is no influence of the dye other than the enhancement of absorption.

Since the amplitudes of both the temperature and the Soret-driven concentration grating are proportional to the absorption coefficient, the independence of A in Fig. 6 on the dye concentration allows also the exclusion of significant electrostrictive contributions [2]. These depend only on the laser intensity, but not on the absorption coefficient, and, hence, would not lead to the straight-line behavior after normalization to the thermal signal.

For polydisperse samples, as the ones discussed here (see below), the weight average Soret coefficient $\langle S_T\rangle_c$ is obtained from the steady-state amplitude [22] of the concentration signal.

2. Diffusion coefficients

a. TDFRS. The diffusion coefficients are obtained from the time dependence of the concentration signal. As with almost all polymeric samples, the nanospheres are not truly monodisperse. For dilute solutions of a polydisperse solute, Eq. (12) becomes [22]

$$\zeta_{het}(t)=1-\frac{(\partial n/\partial c)_{p,T}}{(\partial n/\partial T)_{p,c}}c_0(1-c_0)D_T\sum_k\frac{c_{0,k}}{D_k}(1-\mathrm{e}^{-t/\tau_k}). \quad (14)$$

The molar mass dependence of $S_T=D_T/D$ is attributed completely to D. D_T is taken independent of molar mass, as generally found for polymers in solution [10,8] (see below).

In Ref. [22] it has been shown that TDFRS with step excitation gives the average

$$\langle D\rangle_{c/D}=\frac{\sum_i c_i}{\sum_i c_i/D_i}=\langle D^{-1}\rangle_c^{-1}. \quad (15)$$

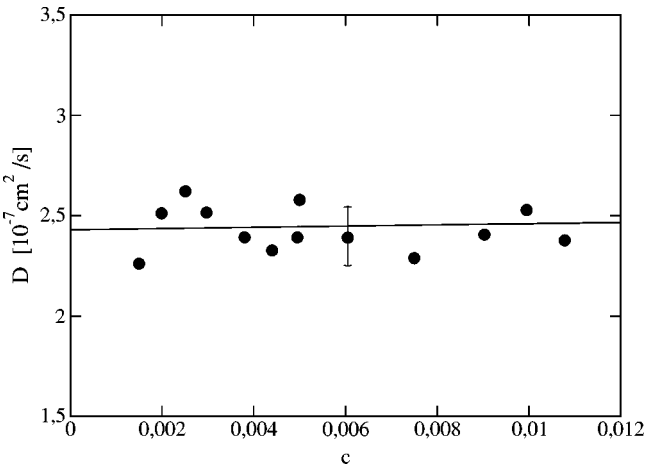

FIG. 7. Diffusion coefficients of $g50/50$ in toluene as measured by TDFRS ($\langle D\rangle_{c/D}$). The solid line corresponds to hard-sphere behavior.

Technically, the CONTIN inversion [25] was used to compute the rate distribution and the average $\langle D\rangle_{c/D}$ from the concentration signal.

Figure 7 shows the diffusion coefficient of $g50/50$ as a function of concentration. The weak concentration dependence is in agreement with the hard-sphere behavior [26]

$$\frac{D}{D_0}=1+1.45\ \phi. \tag{16}$$

$\phi\approx 0.867c$ is the volume fraction of the nanospheres and D_0 the diffusion coefficient extrapolated to zero concentration.

b. PCS. As a consequence of sample polydispersity, the diffusion coefficients measured by photon correlation spectroscopy (PCS) and TDFRS are different [22]. Since the scattered intensity is proportional to cM, PCS gives the z-average diffusion coefficient

$$D_0^{PCS}\equiv\lim_{c\to 0}\langle D\rangle_{cM}=\lim_{c\to 0}\frac{\sum_i c_i M_i D_i}{\sum_i c_i M_i}. \tag{17}$$

c_i is the weight fraction of particles of molar mass M_i. $D_0^{PCS}=1.9\times 10^{-7}$ cm^2/s has been found for $g50/50$. Note that D must also be extrapolated to $q\to 0$ in case of PCS. TDFRS has already been measured at very low $q=6705$ cm^{-1}, rendering the extrapolation obsolete.

Without knowledge of the size distribution and the fractal dimension of the particles, D_0^{PCS} and D_0^{TDFRS} cannot be compared. In principle, the size distribution can be computed from the rate distribution as obtained from the multiexponential decay of the correlation functions in combination with the Stokes-Einstein relation

$$D=\frac{kT}{6\pi\eta_s R}. \tag{18}$$

kT is the thermal energy, η_s the solvent viscosity, and R the particle radius. This requires, however, a high quality of the correlation functions with very little low-frequency noise. Due to the limited quality of the scattering data, we resorted to size exclusion chromatography (SEC) [27], which separates the particles according to their hydrodynamic volume $V_h\propto R^3$. It yields approximately a Gaussian number distribution

$$n(R)=(2\pi\sigma^2)^{-1/2}\ \mathrm{e}^{-(R-R_0)^2/2\sigma^2} \tag{19}$$

with $R_0=(16.0\pm 1.5)$ nm and a width of $\sigma/R_0\approx 0.3$ for $g50/50$. Due to aging effects, the absolute value of R_0 is subject to shifts and less reliable than the normalized width σ/R_0.

If we assume a fractal dimension of 3 for such highly cross-linked spheres, corresponding to $M_i\propto R_i^3$, the ratio D_0^{PCS}/D_0^{TDFRS} can be calculated from Eqs. (15), (17), and (18),

$$\frac{D_0^{PCS}}{D_0^{TDFRS}}=\frac{\sum_i n_i R_i^4\sum_i n_i R_i^5}{\sum_i n_i R_i^3\sum_i n_i R_i^6}=\frac{\langle R^4\rangle_n\langle R^5\rangle_n}{\langle R^3\rangle_n\langle R^6\rangle_n}. \tag{20}$$

Together with the size distribution of Eq. (19) we obtain $D_0^{PCS}/D_0^{TDFRS}\approx 0.9$, which is not too far from the experimental value of $D_0^{PCS}/D_0^{TDFRS}=0.8$.

c. Hydrodynamic radii. The hydrodynmic radii can be obtained from the diffusion coefficients together with the Stokes-Einstein relation [Eq. (18)]. Because of the different averages of the measured diffusion coefficients, the two scattering techniques give an inverse z average in case of PCS and the weight average in case of TDFRS [22],

$$R^{PCS}=\langle R^{-1}\rangle_{cM}^{-1}\approx(19\pm 1)\ \text{nm}, \tag{21}$$

$$R^{TDFRS}=\langle R\rangle_c\approx(15\pm 1)\ \text{nm}.$$

In summary, we find a reasonably consistent picture for the diffusion coefficients and hydrodynamic radii as obtained from the two optical scattering techniques and from SEC.

3. Thermal diffusion coefficients

If the thermal diffusion coefficient of a polydisperse sample does not depend on particle size, as implied by Eq. (14), it can be obtained from the initial slope of the time-dependent concentration signal [22] or from the averages of the Soret and diffusion coefficient according to

$$\langle S_T\rangle_c\langle D\rangle_{c/D}=D_T\langle D^{-1}\rangle_c\langle D\rangle_{c/D}=D_T. \tag{22}$$

$D_T=0.41\times 10^{-7}\text{cm}^2(\text{sK})^{-1}$ is found for $g50/50$ in toluene.

While a molar mass independent D_T has been reported for many different linear polymers [10,8,9], this must not necessarily be true for colloidal particles. Recent thermal field flow fractionation (TFFF) results revealed a size dependence of D_T in aqueous colloidal suspensions [14].

To verify the size independence of D_T for our colloids, some measurements have been performed with another sample of identical chemistry and crosslink density but larger radius ($g50/50b$). The results for the two samples are summarized in Table I. Despite the substantial differences of the diffusion and Soret coefficients, the thermal diffusion

TABLE I. Transport coefficients of $g50/50$ and $g50/50b$ in toluene. The errors are estimated from repeated measurements.

	D^{PCS} 10^{-7} cm^2 s^{-1}	D^{TDFRS} 10^{-7} cm^2 s^{-1}	S_T K^{-1}	D_T 10^{-7} cm^2 (s K)$^{-1}$
$g50/50$	1.9 ± 0.1	2.43 ± 0.15	0.17 ± 0.01	0.41 ± 0.03
$g50/50b$	1.46 ± 0.1	1.57 ± 0.15	0.27 ± 0.02	0.42 ± 0.03

coefficients are identical within the experimental errors, justifying our assumption of a constant D_T.

A constant D_T for swollen colloids in an organic solvent is in agreement with a previous result, where identical D_T has been found for linear polystyrene and highly crosslinked polystyrene microgels [11] in toluene.

A problem not discussed so far is that only a fraction $f \approx 0.05$ of the nanospheres carries gold nuclei, the rest being undoped. Since we have shown in the preceding section that nonlinear feedback is negligible and since we will argue in the next section that D_T is not sensitive to gold doping, this does not change the results and arguments presented in this section.

C. Undoped microgels

For comparison, and to further investigate a potential effect of the gold nuclei, we have also tried to characterize nanospheres in an undoped precursor state. Unfortunately, these particles tend to form aggregates which coexist with the nonaggregated units. We attribute this aggregation tendency to the presence of reactive Si-H groups in the precursor.

The experimental evidence for the aggregates is a bimodal decay of the heterodyne diffraction efficiency in the TDFRS experiments (Fig. 8). The fast process with $D = 2.2\times10^{-7}$ cm^2 s^{-1} is almost identical to the one of the gold-doped microgels. Hence, we attribute it to isolated spheres. The slow one corresponds to a diffusion coefficient $D = 4.5\times10^{-8}$ cm^2 s^{-1} and is most likely caused by aggregates.

Since neither the degree of aggregation nor the thermal diffusion coefficients of the aggregates are known, a unique determination of the Soret and thermal diffusion coefficients of the single spheres and the aggregates is not possible. However, with the plausible assumption of identical D_T and contrast factors $(\partial n/\partial c)_{p,T}$ for the aggregated and nonaggregated colloids, the averaged values $\langle D\rangle_{c/D} = 0.9\times10^{-7}$ cm^2 s^{-1}, $\langle S_T\rangle_c = 0.45$ K^{-1}, and finally $D_T = 0.41\times10^{-7}$ cm^2 (s K)$^{-1}$, can be calculated.

D_T is remarkably close to the value for the doped microgels (Table I). Hence, while not rigorously proven, the assumption of identical D_T for the aggregates and the nonaggregated particles appears justified. Furthermore, the gold nuclei, which are buried inside the colloids and shielded from the solvent by the crosslinked polymer, have no noticeable influence on D_T.

Probably as a consequence of the reactive Si-H-groups, the undoped samples are of limited long-term stability, which manifests itself in a gradual increase of the number and size of the aggregates, a decrease of the number of free colloids, and a slow decrease of $(\partial n/\partial c)_{p,T}$ over several weeks.

V. SUMMARY AND CONCLUSIONS

We have characterized gold-doped polyorganosiloxane microgels with respect to their size distribution, their mass, and thermal diffusion coefficients and their Soret coefficients by means of TDFRS. In addition, translational diffusion and size distribution have been investigated by PCS and SEC, respectively.

A consistent picture has been obtained for the size distribution and the various averages of the diffusion coefficients and hydrodynamic radii as obtained by the optical techniques.

Contrary to colloidal particles in aqueous suspensions, where the thermal diffusion coefficient D_T depends on particle size and mass, D_T does not depend on the size of the microgel. Such a constant D_T is characteristic for linear polymers in organic solvents, but also for crosslinked micro-

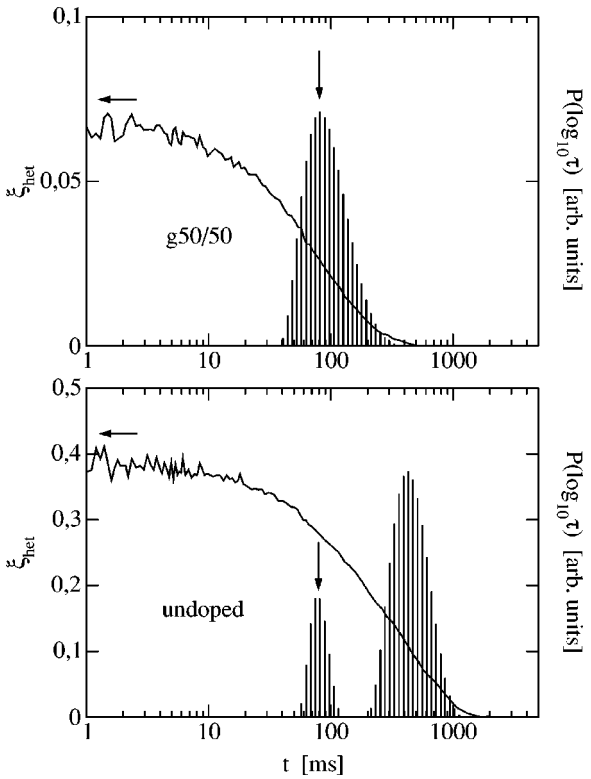

FIG. 8. Concentration part of the heterodyne diffraction efficiency ζ and diffusion-time distribution function $P(\log_{10}\tau)$ for gold-doped ($g50/50$) and undoped ($n50/50$) colloids in toluene. Both $c = 0.0107$. The arrow indicates the nonaggregated species. Note the different scale of the ordinates.

gels in organic and linear polyelectrolytes in aqueous solutions [28]. Because of aggregation phenomena observed for undoped microgels, an unambiguous investigation of the influence of the gold nuclei on D_T has not been possible. A consistent interpretation of the experiments is, however, possible, if we assume identical D_T for the doped, the undoped, and the aggregated particles. This can be rationalized as follows.

Since it could be shown that D_T does not depend on particle size for the doped species, it is also reasonable to assume an aggregation independent D_T for the undoped species. There is no noticeable influence of the gold nuclei on D_T. The gold does not contribute significantly to the total particle mass and is buried inside the polymer and, hence, shielded from the contact with the free solvent on the surface of the particle, where the polymer-solvent interaction responsible for thermal diffusion takes place. A similar behavior has been observed with block copolymers where the monomer units are subject to radial segregation in the polymer-solvent sphere. In these systems, thermal diffusion is dominated by the monomers located in the outer region of the solvation sphere [12].

If the species subject to thermal diffusion absorbs light, there is the possibility for nonlinear Soret feedback, if the temperature gradient is induced by optical absorption. Such feedback is completely irrelevant for TDFRS because of the minute temperature and concentration gradients connected with this technique. The experimental proof is the independence of the amplitude of the concentration signal of the gold-doped system from the addition of dye.

For sample heating along the path of a laser beam inside a thick cell, Soret feedback becomes important already for laser powers of a few mW. This has been analyzed in Ref. [2], and the resulting nonlinear phase shift of the transmitted beam has been employed in Ref. [1]. In principle, this procedure is correct and would yield the Soret coefficient. It suffers, however, from the almost unavoidable convection, which does not allow for the buildup of the stable steady-state concentration modulation. The nonlinear phase shift in Ref. [1] is probably not caused by an escape of the absorbers from the laser beam, which would limit the heat release. Most likely, the transport of cold solution into the beam volume by convection, which also increases with increasing laser power, is responsible for the observed nonlinear phase shift. In light of these arguments, the approximately correct Soret coefficients obtained from the self-induced phase modulation must be viewed as a pure coincidence.

[1] W. Schaertl and C. Roos, Phys. Rev. E **60**, 2020 (1999).
[2] N.V. Tabiryan and W. Luo, Phys. Rev. E **57**, 4431 (1998).
[3] E. Freysz, A. Ponton, P. Delville, and A. Ducasse, Opt. Commun. **78**, 436 (1990).
[4] T. Du and W. Luo, Appl. Phys. Lett. **72**, 272 (1998).
[5] D.W. Pohl, Phys. Rev. A **77**, 53 (1980).
[6] K. Thyagarajan and P. Lallemand, Opt. Commun. **26**, 54 (1978).
[7] W. Köhler, J. Chem. Phys. **98**, 660 (1993).
[8] M.E. Schimpf and J.C. Giddings, J. Polym. Sci., Part B: Polym. Phys. **27**, 1317 (1989).
[9] G. Meyerhoff and K. Nachtigall, J. Polym. Sci. **57**, 227 (1962).
[10] W. Köhler, C. Rosenauer, and P. Rossmanith, Int. J. Thermophys. **16**, 11 (1995).
[11] R. Schäfer, Ph.D. thesis, University of Mainz, 1997.
[12] M.E. Schimpf and J.C. Giddings, J. Polym. Sci., Part B: Polym. Phys. **28**, 2673 (1990).
[13] M. Antonietti, A. Briel, and C. Tank, Acta Polym. **46**, 254 (1995).
[14] S.J. Jeon, M.E. Schimpf, and A. Nyborg, Anal. Chem. **69**, 3442 (1997).
[15] C. Roos *et al.*, Adv. Mater. **11**, 766 (1999).
[16] C. Graf *et al.*, Langmuir **15**, 6170 (1999).
[17] W. Köhler and P. Rossmanith, J. Phys. Chem. **99**, 5838 (1995).
[18] W. Köhler and R. Schäfer, Adv. Polym. Sci. **151**, 1 (1999).
[19] A. Becker, W. Köhler, and B. Müller, Ber. Bunsenges. Phys. Chem. **99**, 600 (1995).
[20] J. Crank, *The Mathematics of Diffusion* (Clarendon, Oxford, 1970).
[21] W. Köhler and P. Rossmanith, Int. J. Polym. Anal. Characterization **1**, 49 (1995).
[22] P. Rossmanith and W. Köhler, Macromolecules **29**, 3203 (1996).
[23] W. Köhler, Entropie **217**, 25 (1999).
[24] W. Köhler and B. Müller, J. Chem. Phys. **103**, 4367 (1995).
[25] S.W. Provencher, Comput. Phys. Commun. **27**, 213 (1982).
[26] B.J. Berne and R. Pecora, *Dynamic Light Scattering* (Wiley, New York, 1976).
[27] G. Glöckner, *Polymer Characterization by Liquid Chromatography* (Elsevier, Oxford, 1987).
[28] R. Spill and W. Köhler (unpublished).